

Design of Photonic Crystal Fiber for 5G Communication Using COMSOL Multiphysics[†]

Sandip Das * and Riya Sen

Geetanjali Institute of Technical Studies, Udaipur 313022, India; riyasen4130@gmail.com

* Correspondence: info.sandipeec@gmail.com

[†] Presented at the 4th International Electronic Conference on Applied Sciences, 27 October–10 November 2023; Available online: <https://asec2023.sciforum.net/>.

Abstract: Photonic crystal fibers (PCFs) have emerged as promising candidates for enabling high-performance 5G communication systems, attributed to their low loss and wide bandwidth characteristics. In this research, we leverage the capabilities of COMSOL Multiphysics v5.6 software to meticulously design a novel photonic crystal fiber (PCF) design based on Topas, featuring a rectangular air gap core with integrated slots, surrounded by a cladding composed of circular and octagon air holes. The circular air holes are arranged in square and octagon lattice structures, while the octagon air holes form a rhombic lattice. The proposed structure exhibits a high birefringence of 0.05 and low effective material loss (EML) of 0.059 cm^{-1} and 0.057 cm^{-1} at 2 THz for x and y polarization mode, respectively. Moreover, the proposed waveguide also has a low confinement loss of 10^{-10} and 10^{-11} cm^{-1} for x and y polarization mode. Thus, the proposed PCF structure exhibits significant potential for facilitating 5G requirements.

Keywords: photonic crystal fiber; 5G communication; terahertz; photonics; optical communication

1. Introduction

The 5G spectrum requires a mix of frequency bands to cater to various use cases. Lower frequency bands (sub-6 GHz) offer wide area coverage and obstacle penetration, while higher frequency bands (millimeter-wave bands like 28 GHz, 39 GHz, and 60 GHz) provide vast spectrum and high data rates but with reduced coverage and susceptibility to blockages. Exploring Terahertz (THz) frequencies, ranging from 0.1 to 10 THz, has become a groundbreaking avenue for enhancing communication capabilities in next-generation wireless networks. Ultra-wideband transmission demands the inclusion of THz or sub-THz bands, resulting in shorter wireless paths and improved fiber penetration. Both wireless and optical technologies play significant roles beyond the 5G communication era.

Terahertz (THz) radiation's extensive frequency range has non-ionizing properties and low energy, making it suitable for penetrating non-polar and non-conductive materials [1]. This characteristic enables diverse applications, including sensing, spectroscopy, medical diagnostics, security screening, imaging, and communication systems [2,3]. Traditional THz systems have been large and relied on free-space propagation, leading to challenges like water vapor absorption loss, material loss, and misalignment between transmitters and receivers [4,5]. To address these issues, waveguides offer a critical solution for low-loss and low-dispersion THz wave propagation.

Waveguides aim to efficiently transmit electromagnetic radiation with minimal loss across various wavelengths. Metallic waveguides suffer from THz radiation absorption and bending losses [6,7]. Dielectric waveguides, like classic optical fibers, show promise for higher frequencies, categorized as solid-, porous-, or hollow-core fibers based on their guiding mechanisms [8]. Solid-core fibers have higher absorption loss than hollow-core fibers [9], but the latter are limited to a narrow frequency band, unlike the broader THz spectrum.



Citation: Das, S.; Sen, R. Design of Photonic Crystal Fiber for 5G Communication Using COMSOL Multiphysics. *Eng. Proc.* **2023**, *56*, 153. <https://doi.org/10.3390/ASEC2023-16309>

Academic Editor: Nunzio Cennamo

Published: 21 November 2023



Copyright: © 2023 by the authors. Licensee MDPI, Basel, Switzerland. This article is an open access article distributed under the terms and conditions of the Creative Commons Attribution (CC BY) license (<https://creativecommons.org/licenses/by/4.0/>).

An alternative approach is the development of photonic crystal fibers (PCFs), wherein a solid core is inserted with micro-structured air holes [10]. The utilization of air as a non-absorbent medium in this fiber design results in several advantageous characteristics, including reduced material loss, enhanced transmission efficiency, and lower bending loss. Moreover, the fiber exhibits high birefringence and offers flexibility in modifying its guiding properties by controlling geometrical parameters.

Researchers extensively studied the optical and chemical properties of various materials for THz waveguides [11]. Commonly employed materials include polymethyl methacrylate, high-density polyethylene plastic, Teflon, Topas, and Zeonex. Topas is preferred due to its low material absorption loss, constant refractive index across a broad frequency range (0.1–2 THz), humidity insensitivity, and versatility in biosensing and photosensitive applications [12,13]. Its compatibility with Zeonex allows for step-index fiber fabrication, making Topas highly promising for advancing THz communication technologies.

Several notable photonic crystal fibers (PC-PCFs) with exceptional guiding properties, including low Effective Mode Loss (EML), low confinement loss, and high-power fraction within porous air holes are studied by different researchers. For instance, a microstructured polymer fiber utilizing a hexagonal array of porous air holes achieved an impressively low EML of 0.018 cm^{-1} at 0.5 THz [14]. Similarly, Uthman et al. proposed another PC-PCF with hexagonal lattice porous air holes, reducing bulk absorption loss of the background material by about 60%. Moreover, Tsuruda et al. introduced a silicon photonic-crystal slab waveguide with a remarkably low propagation loss of 0.04 dB/cm at 0.33 THz.

By exploring and optimizing these PCF waveguide technologies, the efficient and low-loss transmission of THz waves becomes increasingly achievable, opening the door to transformative applications in wireless communication and beyond the 5G era. The paper is organized as follows: In Section 2, the design of the proposed PCF is discussed elaborately. Section 3 presents the results, and finally, the paper is concluded in Section 4.

2. Design of Proposed PCF Structure

The cross-sectional view of the proposed PCF design is shown in Figure 1a. The octagon-shaped air holes form the outer cladding of the rhombic-shaped lattice (lattice 3 and lattice 4), as shown in Figure 1b. The diameter of the inner circular air hole adjacent to the core is d_1 and the circular air hole in the exterior layer has a diameter d_2 . The inner air holes form a square lattice (lattice 2), and the outer air holes are arranged in an octagonal-shaped lattice (lattice 1), as shown in Figure 1b. The core consists of 13 rectangular slots of air holes, which form the shape of an octagon having a diameter d_{core} . The dimension of the rectangular air holes has a length 'L' and width 'W', and each rectangular slot is separated by a distance known as pitch ' Λ '. Except for the three center slots with length 'L' and four slots at the end (on both sides) with length ' L_4 ', the length of each of the remaining rectangular slots reduces on either side. The length of the rectangular slots decreasing on either side is represented as L_1 , L_2 , and L_3 . Four rectangular slots of length ' L_4 ' and width 'W' are placed in between two octagon-shaped air holes above and below the core, as shown in Figure 1a. The dimensions are listed in Table 1.

Table 1. Dimension of the proposed PCF air holes.

| Shape | Dimension |
|---|--|
| Inner air hole diameter, d_1 | 90 μm |
| Outer air hole diameter, d_2 | 76 μm |
| Core diameter, d_{core} | 180 μm |
| pitch, Λ | 5 μm |
| Width of rectangular core, W | 10 μm |
| Length of rectangular slots, L_1, L_2, L_3, L_4 | 140 μm , 120 μm , 100 μm , 60 μm |

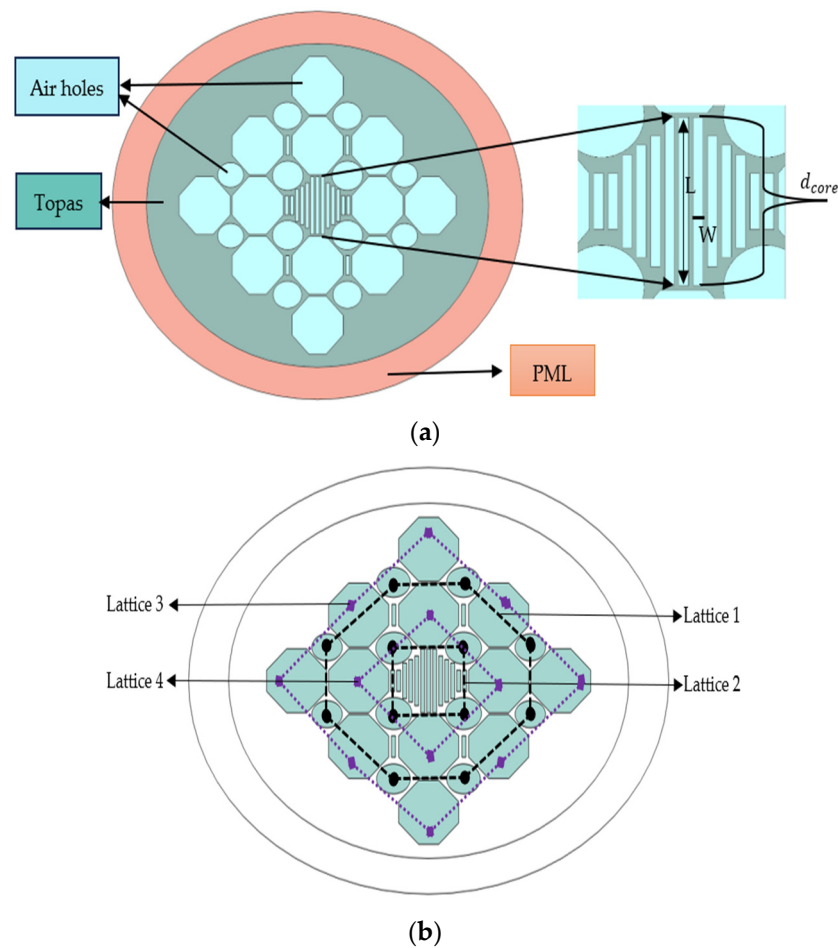


Figure 1. Proposed structure of PCF. (a) Cross-section view of the proposed PCF; (b) representation of lattice formed by circular air holes and octagon air holes.

The finite element method (FEM)-based COMSOL v5.6 software is used to simulate the proposed PCF. For the entire simulation process user-controlled mesh is selected for utmost precision. The entire structure was represented by 14,382 triangular components and 220 vertex elements. In order to map the varying diameters of the air holes, the minimum element size was set at $0.09 \mu\text{m}$. The minimum element quality obtained is 0.3914. The mesh representation of the structure is shown in Figure 2.

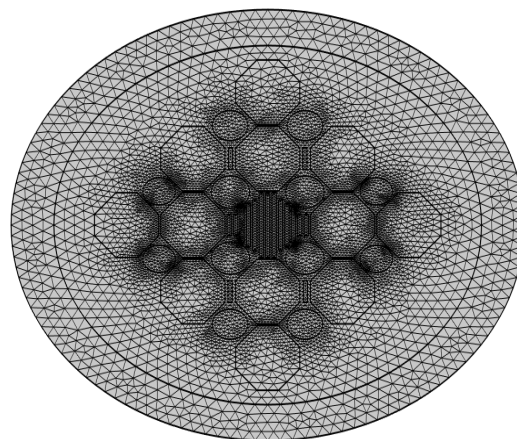


Figure 2. Mesh representation of the proposed PCF structure.

The cladding region of the PCF is surrounded by a protective layer that uses the Perfectly Matched Layer (PML) boundary condition. This layer not only ensures simulation accuracy but also effectively eliminates ambient reflections, improving results precision. The structure’s background material is topaz, with a refractive index of 1.528 that remains constant throughout a frequency range of 0.1–2 THz.

3. Results and Discussions

The proposed PCF is numerically analyzed by utilizing the finite element method. Various PCF characteristics, namely birefringence, effective refractive index, effective material loss (EML), confinement loss (CL), effective area and V-parameter, and dispersion properties, are analyzed to study the performance of the PCF in the THz range. In Figure 3, the profiles for mode field covering both x-pol and y-pol are represented.

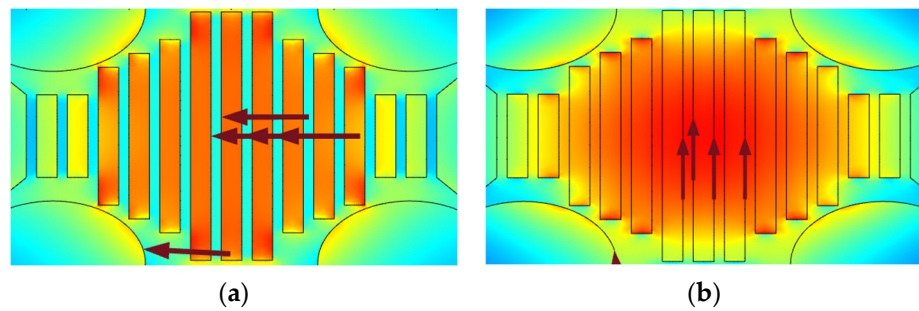


Figure 3. Fundamental mode field distributions of the proposed PCF at 1 THz (a) x-pol (b) y-pol.

3.1. Effective Refractive Index

The effective refractive index of the proposed PCF in correlation with the frequency is depicted in Figure 4 for both x-pol and y-pol. As the frequency increases, the fiber’s effective refractive index also rises, as shown in Figure 4a. Higher frequencies cause the mode power to extend into the cladding region, further increasing the effective refractive index. At 2 THz, the suggested fiber exhibits effective refractive indices of approximately 1.1014 for x-polarization and 1.1537 for y-polarization. It is found that the effective refractive index for y-polarization is higher when compared to x-polarization. The y-polarization is chosen as the primary mode since the confinement of light in the core is stronger.

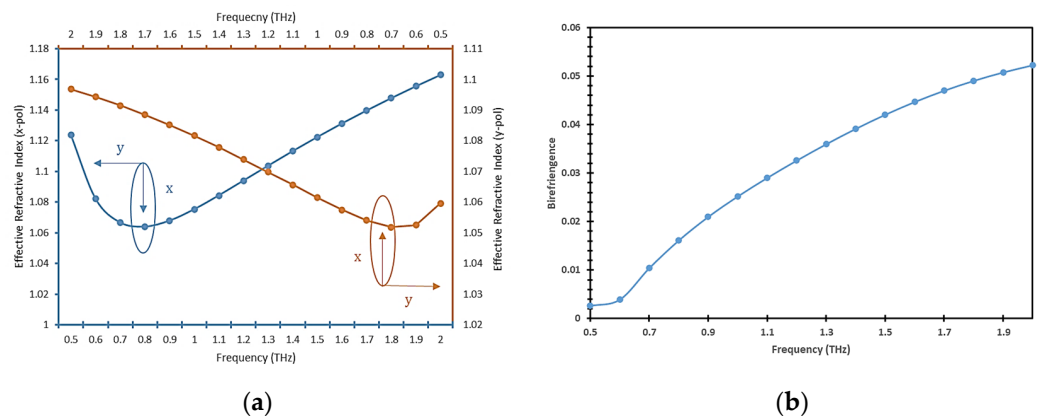


Figure 4. Graphical representation of (a) effective refractive index vs. frequency for x-pol and y-pol and (b) birefringence versus frequency.

3.2. Birefringence

The difference between the refractive indices of two orthogonally polarized modes is termed birefringence, and it is expressed using the following equation.

$$B = |\eta_x - \eta_y| \tag{1}$$

where B represents birefringence and η_x and η_y represents the respective refractive index of x and y polarised modes. From Figure 4b, it is clearly seen that birefringence rises with the increase in frequency up to 1.5 THz and starts to reduce or flatten after 1.5 THz. The higher refractive index gap between the core and the cladding can explain the rise in effective refractive index at high frequencies.

3.3. Effective Material Loss and Confinement Loss

Terahertz waves propagating through the PCF mostly suffer from effective material loss (EML), simply known as material absorption loss (α_{eff}). The EML for the proposed PCF can be expressed as follows:

$$\alpha_{eff} = \sqrt{\frac{\epsilon_0}{\mu_0}} \left(\frac{\int_{mat} \eta_{mat} |E|^2 \alpha_{mat} dA}{|\int_{all} S_z dA|} \right) \tag{2}$$

where ϵ_0 and μ_0 are the relative permittivity and permeability of the vacuum, η_{mat} is the refractive index of the material and α_{mat} denotes the absorption loss of the bulk material. S_z denotes the z-component of the Poynting vector, which is in the direction of the electromagnetic wave transmission. From Figure 5 it is seen that the EML keeps rising with the increase of frequency. It is seen from the figure that for the x-polarization mode, EML is more compared to the y-polarization mode as the frequency increases. In both the modes EML is less for lower frequencies as the confinement of EM wave is more concentrated in the core.

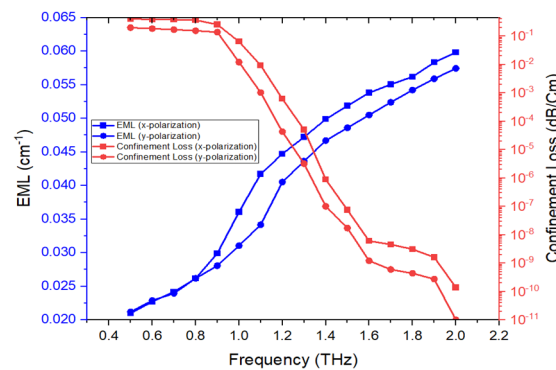


Figure 5. EML and confinement loss of x-pol and y-pol mode versus frequency.

Confinement loss is a crucial parameter in any PCF design. The mathematical representation below illustrates how light loss can occur in the core region due to the specific structure of the photonic crystal fiber (PCF), which includes air holes within the cladding. The following equation shows the relationship between the velocity of light in the waveguide, frequency, and the imaginary part of the effective refractive index.

$$\alpha_{CL} = 8.686 \times \frac{2\pi f}{c} \times Im(\eta_{eff}) \tag{3}$$

From the above figure, it can be understood that as the frequency increases, the confinement loss reduces, indicating that the confinement of light in the core region is stronger. The minimum confinement loss obtained is 10^{-10} cm^{-1} and 10^{-11} cm^{-1} for x-polarization and y-polarization modes.

4. Conclusions

In conclusion, this research article introduces a novel design of a Topas-based photonic crystal fiber (PCF) with a rectangular air gap core containing slots surrounded by cladding comprised of circular and octagon air holes. The arrangement of circular air holes forms a square and octagon lattice structure, while the octagon air holes create a rhombic lattice. The primary objectives of this study were to achieve an ultra-low effective mode area (EML), high birefringence, and very low confinement loss, all tailored to specific frequency ranges. The proposed PCF structure shows great promise for 5G applications due to its unique combination of properties and functionalities. In the future, more waveguide properties like core power fraction, dispersion, spot size, and V-parameter can be studied in connection to varying core diameters and porosity to gauge the performance in a much better way.

Author Contributions: S.D. was responsible for generating concepts, conducting simulations, and preparing the initial draft of the paper. R.S. took on the role of optimizing the simulated design, editing the paper, and preparing the final draft. Ultimately, S.D. and R.S. collaborated to finalize the paper. All authors have read and agreed to the published version of the manuscript.

Funding: This research received no external funding.

Institutional Review Board Statement: Not applicable.

Informed Consent Statement: Not applicable.

Data Availability Statement: Data are contained within the article.

Conflicts of Interest: The authors declare no conflicts of interest.

References

1. Carr, G.L.; Martin, M.C.; McKinney, W.R.; Jordan, K.; Neil, G.R.; Williams, G.P. High-power terahertz radiation from relativistic electrons. *Nature* **2002**, *420*, 153–156. [[CrossRef](#)] [[PubMed](#)]
2. Pinto, A.M.R.; Lopez-Amo, M. Photonic Crystal Fibers for Sensing Applications. *J. Sens.* **2012**, *2012*, 598178. [[CrossRef](#)]
3. Zhang, J.; Grischkowsky, D. Waveguide terahertz time-domain spectroscopy of nanometer water layers. *Opt. Lett.* **2004**, *29*, 1617–1619. [[CrossRef](#)] [[PubMed](#)]
4. Skorobogatiy, M.; Dupuis, A. Ferroelectric all-polymer hollow Bragg fibers for terahertz guidance. *Appl. Phys. Lett.* **2007**, *90*, 113514. [[CrossRef](#)]
5. Hasan, R.; Anower, S.; Islam, A.; Razzak, S.M.A. Polarization-maintaining low-loss porous-core spiral photonic crystal fiber for terahertz wave guidance. *Appl. Opt.* **2016**, *55*, 4145–4152. [[CrossRef](#)] [[PubMed](#)]
6. Nagatsuma, T.; Ducournau, G.; Renaud, C. Advances in terahertz communications accelerated by photonics. *Nat. Photon.* **2016**, *10*, 371–379. [[CrossRef](#)]
7. Atakaramians, S.; Afshar, S.; Monroe, T.M.; Abbott, D. Terahertz dielectric waveguides. *Adv. Opt. Photonics* **2013**, *5*, 169–215. [[CrossRef](#)]
8. Dupuis, A.; Stoeffler, K.; Ung, B.; Dubois, C.; Skorobogatiy, M. Transmission measurements of hollow-core THz Bragg fibers. *J. Opt. Soc. Am. B* **2011**, *28*, 896–907. [[CrossRef](#)]
9. Nagel, M.; Marchewka, A.; Kurz, H. Low-index discontinuity terahertz waveguides. *Opt. Express* **2006**, *14*, 9944–9954. [[CrossRef](#)] [[PubMed](#)]
10. Uthman, M.; Rahman, B.M.A.; Kejalakshmy, N.; Agrawal, A.; Grattan, K.T.V. Design and Characterization of Low-Loss Porous-Core Photonic Crystal Fiber. *IEEE Photon. J.* **2012**, *4*, 2315–2325. [[CrossRef](#)]
11. Islam, S. Design and Analysis of Advanced Photonic Devices for Electromagnetic Transmission and Sensing. Ph.D. Thesis, Faculty of Engineering, University of Adelaide, Adelaide, Australia, 2021.
12. Hasan, M.R.; Islam, M.A.; Rifat, A.A. A single mode porous-core square lattice photonic crystal fiber for THz wave propagation. *J. Eur. Opt. Soc.-Rapid Publ.* **2016**, *12*, 15. [[CrossRef](#)]
13. Hasan, R.; Islam, A.; Anower, M.S.; Razzak, S.M.A. Low-loss and bend-insensitive terahertz fiber using a rhombic-shaped core. *Appl. Opt.* **2016**, *55*, 8441–8447. [[CrossRef](#)] [[PubMed](#)]
14. Hasan, R.; Akter, S.; Khatun, T.; Rifat, A.A.; Anower, S. Dual-hole unit-based kagome lattice microstructure fiber for low-loss and highly birefringent terahertz guidance. *Opt. Eng.* **2017**, *56*, 043108. [[CrossRef](#)]

Disclaimer/Publisher's Note: The statements, opinions and data contained in all publications are solely those of the individual author(s) and contributor(s) and not of MDPI and/or the editor(s). MDPI and/or the editor(s) disclaim responsibility for any injury to people or property resulting from any ideas, methods, instructions or products referred to in the content.